Official journal of the American Society of Gene & Cell Therapy

MTOpen

In Vivo CRISPR/Cas9 Gene Editing Corrects Retinal Dystrophy in the S334ter-3 Rat Model of Autosomal Dominant Retinitis Pigmentosa

Benjamin Bakondi[1], Wenjian Lv[1,2], Bin Lu[1], Melissa K Jones[1], Yuchun Tsai[1], Kevin J Kim[1], Rachelle Levy[1], Aslam Abbasi Akhtar[1], Joshua J Breunig[1], Clive N Svendsen[1] and Shaomei Wang[1]

[1]*Board of Governors Regenerative Medicine Institute, Department of Biomedical Sciences, Cedars-Sinai Medical Center, Los Angeles, California, USA;* [2]*Current address: Department of Stem Cell and Regenerative Biology, Harvard University, Cambridge, Massachusetts, USA*

Reliable genome editing via Clustered Regularly Interspaced Short Palindromic Repeat (CRISPR)/Cas9 may provide a means to correct inherited diseases in patients. As proof of principle, we show that CRISPR/Cas9 can be used *in vivo* to selectively ablate the rhodopsin gene carrying the dominant S334ter mutation (*Rho*^{S334}) in rats that model severe autosomal dominant retinitis pigmentosa. A single subretinal injection of guide RNA/Cas9 plasmid in combination with electroporation generated allele-specific disruption of *Rho*^{S334}, which prevented retinal degeneration and improved visual function.

Received 29 September 2015; accepted 5 December 2015; advance online publication 19 January 2016. doi:10.1038/mt.2015.220

INTRODUCTION

Gene replacement strategies in clinical trials for retinal degenerative diseases were designed to compensate for the biallelic inheritance of recessive, loss-of-function mutations.[1] This approach, however, is inapplicable to autosomal dominant retinitis pigmentosa (adRP) in which disease penetrance is conferred by a monoallelic, gain-of-function mutation.[2] Twenty-four genes have been implicated in adRP etiology, with *Rho* variations constituting the highest proportion of RP cases.[3] Studies in transgenic animals bearing dominant *Rho* mutations showed that disease severity can be mitigated by silencing the mutant RNA transcript[4,5] or via transcriptional suppression using an allele-independent approach to target both mutant and wild-type genes.[6] The caveat to these approaches, however, is the requisite supplementation with the wild-type *Rho* (*Rho*^{WT}) transcript.

Allele-specific genomic ablation using Clustered Regularly Interspaced Short Palindromic Repeat (CRISPR)/Cas9 may present a simplified therapeutic strategy in which retinal function is restored by the remaining *Rho*^{WT} allele in adRP patients. Though two *Rho*^{WT} alleles will remain following transgene ablation in the model used here, patient hemizygosity does not manifest in haploinsufficiency as *Rho*^{WT} expression between 50 and 200% is clinically asymptomatic.[2] Moreover, as little as 10% of total *Rho* expression from a control transgene was shown to be sufficient to reconstitute the WT phenotype in *Rho* knockout mice.[7] Accordingly, adRP may be amenable to allele-specific ablation therapy without requiring exogenous *Rho*^{WT} supplementation.

Transgenic S334ter rats that possess the mouse genomic fragment containing *Rho*^{S334} show phenotypic similarity to human class-I RHO mistrafficking mutations, exhibiting continual photoreceptor (PR) loss and commensurate vision decline.[8] The S334ter mutation generates a serine substitution at amino acid position 334/338 for a stop codon resulting in early termination ("ter"), and RHO truncation by 15 C-terminal residues.[3] The resultant peptide (RHO^{S334}) lacks three serines required for PR deactivation following light stimulation,[9] and part of the signal sequence required for RHO trafficking to photoreceptor outer segments (POS).[10] The morphological development of POS is critical to support phototransduction[11] and is absent in line-3 S334ter rats (S334ter-3).[12] As RHO constitutes ~85% of the total protein content in PRs, its retention in processing organelles at the cell body instigates PR toxicity and is compounded by constitutive PR activity, resulting in apoptosis.[13]

We hypothesized that the selective ablation of *Rho*^{S334} *in vivo* would eliminate the RHO^{S334} production and toxicity and allow native *Rho*^{WT} to restore the phenotype to that of the nondystrophic retina. We used CRISPR/Cas9 to selectively disrupt *Rho*^{S334} by utilizing the requirement of Cas9 activity on the recognition of a protospacer adjacent motif (PAM) present in *Rho*^{S334}, which diverges from the *Rho*^{WT} sequence by one nucleotide (5′-TG*G*-3′ versus 5′-TG*C*-3′, respectively). Here, we show that this single base pair difference facilitated discrimination between *Rho* alleles during Cas9 cleavage, which permitted the unabated function of *Rho*^{WT} to prevent RP pathology and loss of visual acuity.

RESULTS

Differential distribution of RHO^{S334} versus RHO^{WT} in S334ter-3 rats

S334ter-3 rats are characterized by the rapid and progressive loss of PRs in the outer nuclear layer (ONL) beginning at postnatal day (P) 11, until complete degeneration is reached by P28, at which time just a single row of PR nuclei remain.[12] Similarly, S334ter-3 rat retinas showed near full ONL thickness

The first two authors contributed equally to this work.

Correspondence: Shaomei Wang, Cedars-Sinai Medical Center, 8700 Beverly Blvd., AHSP-A8108, Los Angeles, California 90048, USA.
E-mail: shaomei.wang@cshs.org

at P14 (**Supplementary Figure S1a**, bracketed areas), compared with a single discontinuous row of remaining PR nuclei at P33 (**Supplementary Figure S1c**, bracketed areas). As previously described for line-4 S334 rats, RHO N-terminal immunolabel identified both the truncated (RHO^{S334}) and full-length (RHO^{WT}) isoforms. However, RHO C-terminal-specific immunolabel exclusively identified the RHO^{WT} isoform.[14] Immunolabeled N-terminal RHO in P14 S334ter-3 retinas was predominantly mislocalized at PR cell bodies throughout the ONL, while RHO^{WT} was present in the ONL and polarized toward PR inner segments (**Supplementary Figure S1a** versus **S1b**). The consequence of RHO mistrafficking by P33 was the degeneration of PRs in the ONL, which consisted of a single discontinuous layer of PR nuclei (**Supplementary Figure S1c,d**).

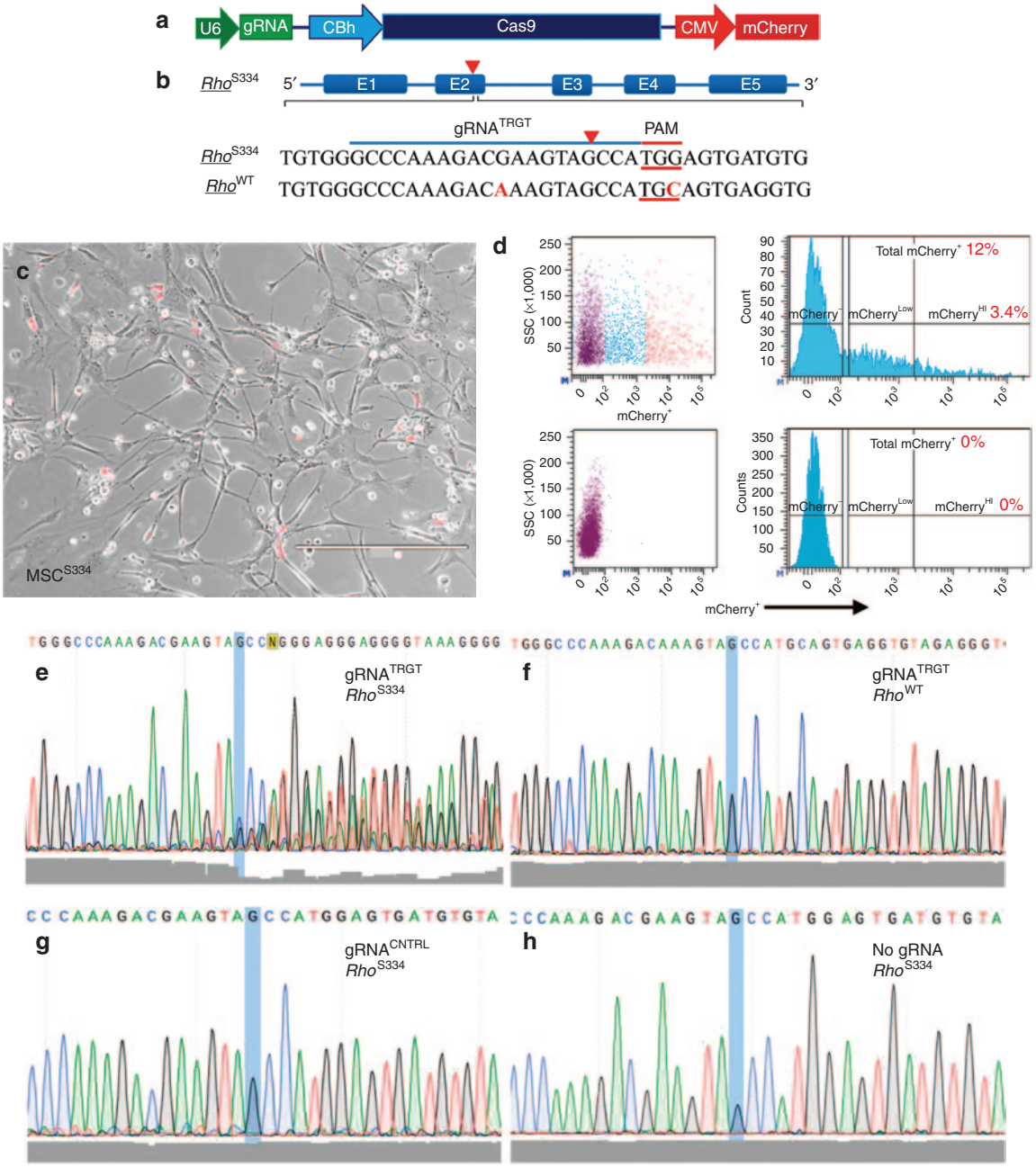

Figure 1 Allele-specific targeting and disruption of *Rho*^{S334} *in vitro*. (**a**) Schematic of px330 construct used. (**b**) $gRNA^{TRGT}$ and predicted genomic DNA binding sites in Rho^{S334} and Rho^{WT}. PAM (red underlined bases) and mismatches (red font) are shown. (**c**) Phase contrast photomicrograph of mCherry$^+$ and mCherry$^-$ $MSCs^{S334}$ 3-days post-lipofection with gRNA constructs prior to fluorescence-activated cell sorting (FACS) isolation. (**d**) FACS gating strategy for mCherry$^+$ MSC^{S334} isolation is shown. mCherry$^+$ cells represented 12% of the total population, with the brightest 3.4% mCherry$^+$ $MSCs^{S334}$ selected for genomic DNA sequence analysis using PCR amplicons encompassing predicted Cas9 cleavage sites. (**e–h**) Genomic DNA sequencing results are shown with Phred quality scores (gray shading) at bottom. DNA disruption is shown from $gRNA^{TRGT}$-transfected $MSCs^{S334}$ downstream from the Cas9 cleavage site (blue highlight) in Rho^{S334} (e), but not in Rho^{WT} (f). Genomic disruption was absent at the Rho^{S334} locus using $gRNA^{CNTRL}$ (g) or with no vector in untreated eyes (h). Bar = 400 µm. CMV, cytomegalovirus; MSC, mesenchymal stem cell; PAM, protospacer adjacent motif.

Guide RNA vector design and strategy

We designed a 20 nucleotide targeting-guide RNA (gRNA) construct (gRNA^{TRGT}) complementary to a region in exon 1 immediately upstream of a PAM unique to the *Rho*^{S334} locus in order to discriminate alleles during Cas9 cleavage (**Figure 1a**,**b**). The homology between mutant and WT *Rho* alleles at the gRNA binding locus differs by one nucleotide at position 10/20 (**Figure 1b**). gRNA^{TRGT} targeted the second of four PAMs identified as unique to *Rho*^{S334} to give the greatest probability for allele-specific ablation. We reasoned that 3′ open reading frame disruptions downstream to the two PAMs in exon 4 risked generating further truncated RHO isoforms, while targeting the 5′-most PAM of exon 1 risked *Rho*^{S334} open reading frame restoration as a consequence of polymerase skipping. While the S334ter mutation was not the target of our gRNA^{TRGT}, dominant adRP mutations have been identified in patients that generated novel PAM sequences[15] that may be targetable similar to the current strategy (**Supplementary Table S1**).

Rho^{S334} disruption *in vitro*

RhoS334-selective cleavage with gRNA^{TRGT} was confirmed in cultured bone marrow-derived stromal cells derived from S334ter-3 rats (MSCs^{S334}). mCherry^{+} MSCs^{S334} were isolated by fluorescence-activated cell sorting 3 days after transfection (**Figure 1c**,**d**), and PCR-amplified regions of genomic DNA that encompassed the predicted Cas9 cleavage sites were sequenced. Multiple peaks and decreased nucleotide read fidelity (Phred quality scores) indicated the presence of novel genomic sequences originating downstream from the disparate PAM of *Rho*^{S334}, which was absent at the homologous *Rho*^{WT} locus (**Figure 1e**,**f**). Genomic disruption was not observed using a second gRNA that targeted exon 2 of *Rho*^{S334}, which had four nucleotide mismatches from *Rho*^{WT}, and was thus used as a control gRNA (gRNA^{CNTRL}) for *in vivo* experiments (**Figure 1g**). Likewise, genomic disruption was not observed in cells from untreated retinas (**Figure 1h**).

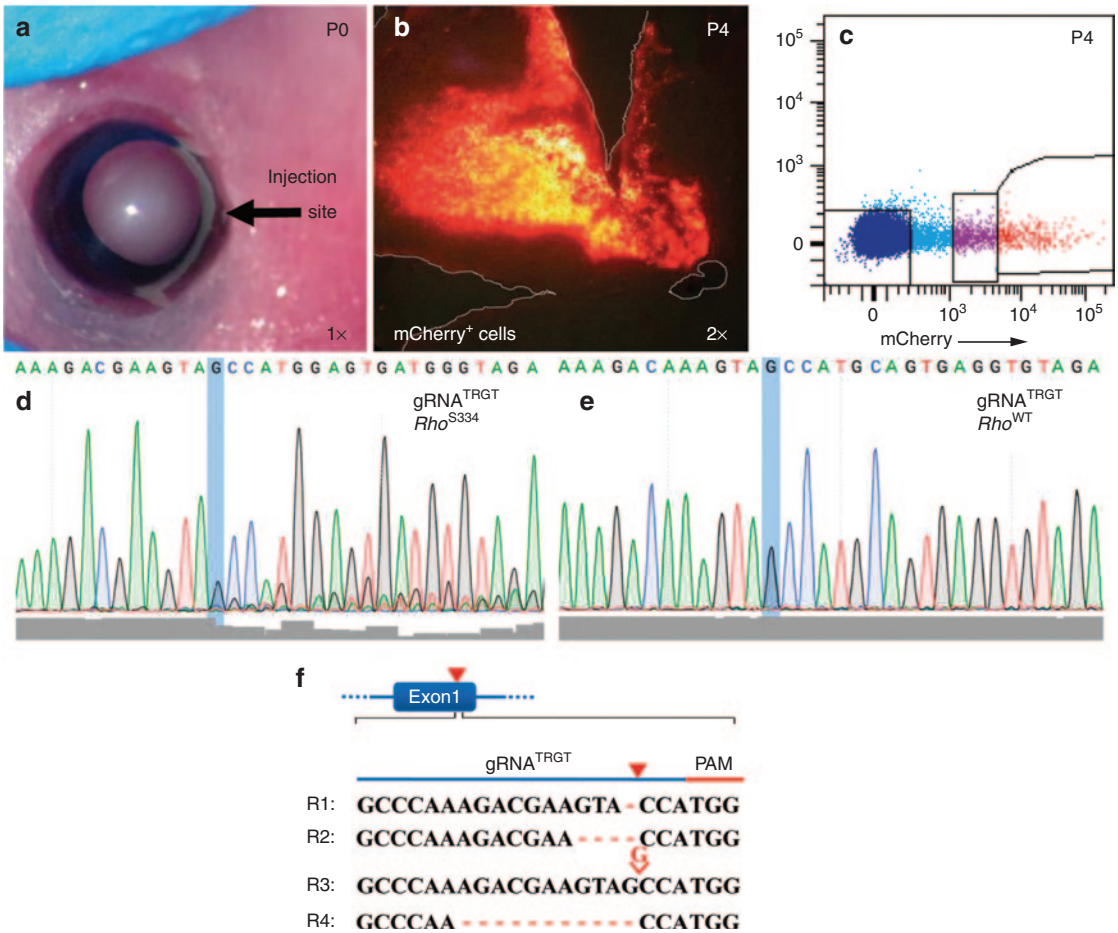

Figure 2 Allele-specific targeting and disruption of *Rho*^{S334} *in vivo*. (**a**) Fast-Green DNA dye shows plasmid distribution following unilateral subretinal injection in S334ter-3 rats at P0. (**b**) Representative retinal flat-mount shows variable mCherry intensity and uneven distribution 4 days after injection. (**c**) Gating strategy for fluorescence-activated cell sorting isolation of enzymatically dissociated P4 retinal cells with mCherry fluorescence intensity at high (red, 0.3%) intermediate (purple, 0.6%), and no (blue, 97.9%) expression. Sanger sequencing of PCR-amplified genomic *Rho* loci from photoreceptors showed *in vivo* disruption of *Rho*^{S334} (**d**), but not *Rho*^{WT} (**e**) using gRNA^{TRGT}. (**f**) *Rho*^{S334} locus targeting schematic and deep sequencing reads shows insertions/deletions (indels) proximal to the predicted cleavage site (arrowhead) from gRNA^{TRGT}-expressing cells. PAM, protospacer adjacent motif.

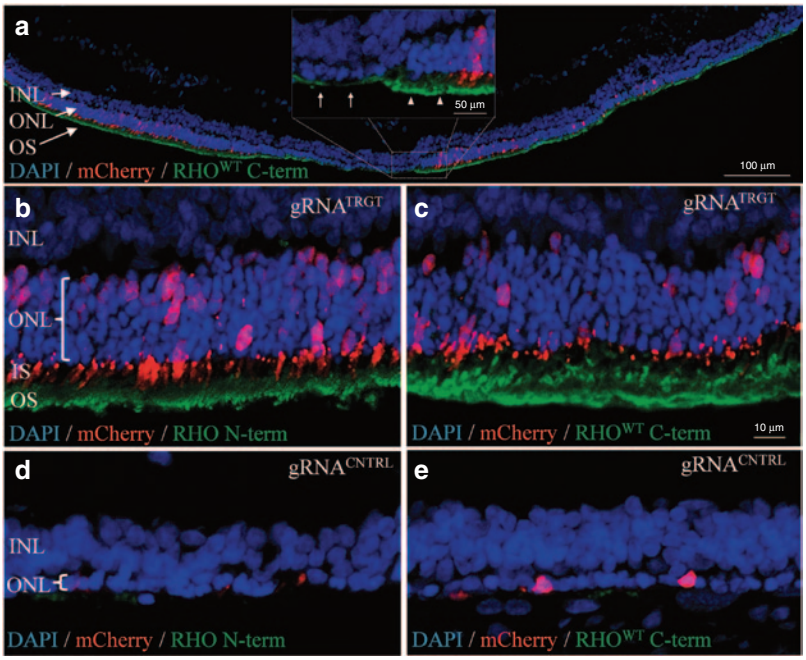

Figure 3 Phenotypic rescue by *Rho*^{S334}-selective ablation. (**a**–**e**) Fluorescent confocal images of gRNA^{TRGT}-treated (**a**–**c**) and gRNA^{CNTRL}-treated (**d**,**e**) retinas at P33. (**a**) Montage image shows that mCherry distribution correlated with ONL rescue (DAPI, blue) and POS formation (RHO^{WT} C-terminal immunolabel, green). Inset: magnified image of outlined region shows preserved ONL with organized POS (arrowheads) adjoining degenerated ONL with diminished POS (arrows). (**b**,**c**) RHO N-terminal (**b**) and C-terminal (**c**) immunostaining in gRNA^{TRGT}-treated retinas was absent from PR cell bodies and localized to OS. Significant PR preservation in the ONL was observed from gRNA^{TRGT} treatment (**b**, bracketed areas). (**d**,**e**) RHO N-terminal (**d**) and C-terminal (**e**) immunostaining was absent in gRNA^{CNTRL}-treated retinas, which lacked POS formation and ONL contained one row of remaining PR nuclei (**d**, bracketed areas). DAPI, 49,69-diamidino-2-phenylindole; INL, inner nuclear layer; IS, inner segment; ONL, outer nuclear layer; OS, outer segment; POS, photoreceptor outer segment; PR, photoreceptor.

Rho^{S334} disruption *in vivo*

To evaluate *Rho*^{S334} disruption *in vivo*, S334ter-3 rats received a single unilateral subretinal injection of the gRNA^{TRGT} construct at P0 (**Figure 2a**), immediately followed by electroporation in order to facilitate plasmid uptake by PRs in cell cycle.[16] Retinas were dissociated at P4 and plasmid-transfected cells were sorted on the basis of mCherry expression (**Figure 2b**,**c**), followed by genomic DNA extraction for Sanger sequencing. We confirmed multiple genomic sequences resulting from *Rho*^{S334}-selective cleavage downstream the Cas9 cleavage site (blue highlight) in P4 mCherry^{+} PRs (**Figure 2d**), but no cleavage was detected at the *Rho*^{WT} locus (**Figure 1e**). Genomic cleavage was similar in PRs that expressed mCherry at high (mCherry^{Hi}) or intermediate/low (mCherry^{Lo}) levels in three rats (**Supplementary Figure S2**). PCR-amplified genomic DNA regions encompassing the gRNA^{TRGT} target site were further sequenced after clonal expansion in NEB-α to determine indel frequency. The ratio of clones in which indels were detected from two rats represented cleavage efficiencies of 33% (7/21 clones) and 36% (15/42 clones). Indels were not detected at the *Rho*^{WT} locus or the next 8 motif-mismatch-predicted off-target loci (**Supplementary Table S2**). Similarly, histological evaluation using cresyl violet stain showed phenotypic rescue by gRNA^{TRGT} treatment compared with the contralateral untreated eye of the same animal (**Supplementary Figure S3a**,**c** versus **S3b**,**d**).

PR preservation following *Rho*^{S334} ablation

To determine whether the retinal phenotype was altered in S334ter-3 rats, gRNA^{TRGT} and gRNA^{CNTRL} treatments were assessed by immunohistology at P33. Extensive and robust retinal preservation was observed in gRNA^{TRGT}-injected eyes with up to eight layers of rescued PRs, in sharp contrast to the single PR layer in gRNA^{CNTRL}-treated retinas (**Figure 3a**–**c** versus 3d,e). PR rescue was observed exclusively in transfected regions demonstrated by coincident mCherry expression, which were the only regions with observable POS formation, morphologically characteristic of the WT phenotype that was absent in gRNA^{CNTRL}-injected eyes (**Figure 3d**,**e**). Furthermore, N-terminal RHO labeling confirmed the absence of RHO^{S334} from PR cell bodies in the rescued ONL (**Figure 3b**), while C-terminal labeling showed RHO^{WT} to be strictly confined to POS (**Figure 3c**). These data suggest that *Rho*^{S334} was ablated and the toxic effect of RHO^{S334} was removed in transfected regions, which subsequently permitted proper RHO^{WT} trafficking, POS formation, and PR survival. gRNA^{CNTRL}-treated retinas lacked appreciable amounts of either RHO isoform at P33 due to extensive degeneration (**Figure 3d**,**e**).

Retinal synapse preservation following *Rho*^{S334} ablation

Immunostaining of degenerated gRNA^{CNTRL}-treated retinas revealed that the single layer of remaining PRs were non-*Rho*-expressing cone cells (**Figure 4a**,**d**), the morphology of which was well preserved with gRNA^{TRGT} treatment (**Figure 4e**,**h**). mCherry fluorescence intensity in PRs appeared highest in mitochondria-rich inner segments (**Figure 4g**). In addition, gRNA^{TRGT} treatment preserved the dendritic arborization of rod-bipolar cells (protein kinase C-α, **Figure 4i**) and synaptic density between second-order

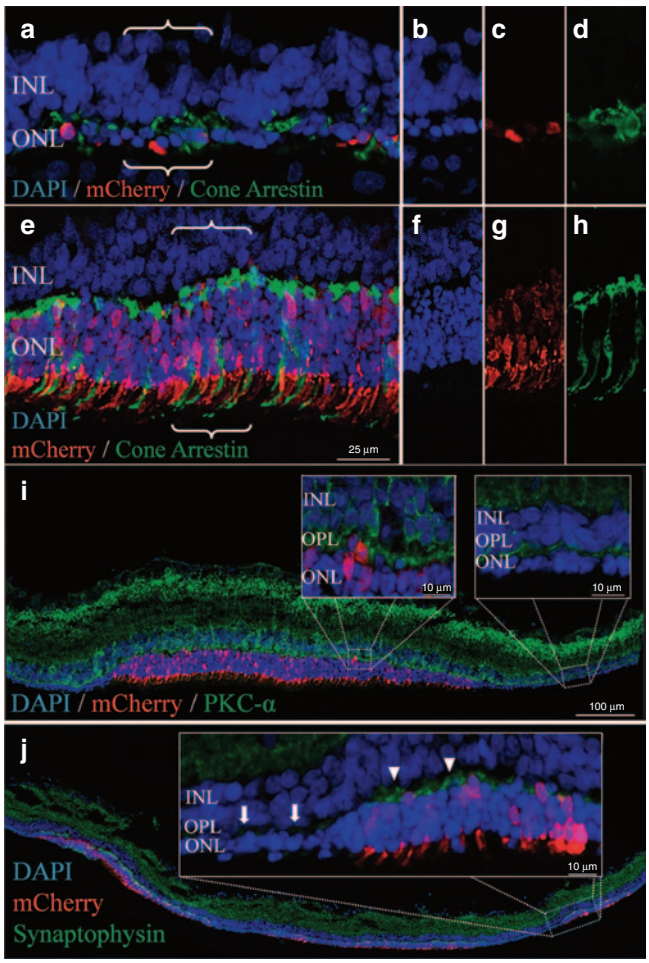

Figure 4 *Rho*^{S334} ablation preserved cone morphology and second-order retinal neuron synapses. Fluorescence confocal microscopy images from gRNA^{CNTRL}-treated (**a–d**) or gRNA^{TRGT}-treated (**e–j**) eyes at P33. (**a**,**b**) Surviving PRs after gRNA^{CNTRL} treatment were non-*Rho*-expressing cones PRs (**a**,**d**, cone arrestin, green), which lacked typical morphological features observed in retinas rescued with gRNA^{TRGT} treatment (**e**,**h**). Individual channel images corresponding to bracketed areas in (**a**) and (**e**) show rescued PR nuclei (DAPI, (**b**) versus (**f**)) in gRNA vector transfected areas (mCherry, (**c**) versus (**g**)) with preserved cone morphology (*i.e.*, pedicles and POS, (**d**) versus (**h**)). (**i**) Greater dendritic arborization of INL-resident rod-bipolar neurons (PKC-α, green) was evident at the OPL in mCherry^{+} areas following gRNA^{TRGT} treatment (left inset), in contrast to the adjacent degenerated area lacking mCherry^{+} (right inset). (**j**) Similarly, synaptophysin immunolabel (green) showed greater intensity in OPL regions in which PR nuclei preservation (DAPI) corresponded with mCherry^{+} expression (inset: arrowheads), in sharp contrast with the adjacent unprotected area to which gRNA^{TRGT} transfection did not extend (inset: arrows). DAPI, 49,69-diamidino-2-phenylindole; INL, inner nuclear layer; ONL, outer nuclear layer; OPL, outer plexiform layer; PKC-α, protein kinase C-alpha; PR, photoreceptor.

inner retinal neurons and PRs within rescued retinal areas (synaptophysin; **Figure 4j**), compared with adjoining degenerated areas.

Quantification of PR density and visual function in *Rho*^{S334}-treated retinas

The extent of mCherry distribution in retinal flat-mounts at P33 reached 29% maximal area coverage, with uneven fluorescence intensity in transfected regions (**Figure 5a**). By cross-section analysis, the density of PRs in mCherry^{+} regions from gRNA^{TRGT} treatment at P33 was 307 ± 82 PR nuclei/100 µm or ninefold greater than from gRNA^{CNTRL} treatment (33 ± 3 nuclei/100 µm, $P \leq 0.01$) and was similarly higher when compared with comparable regions (nonfluorescent) of untreated control (27 ± 13 nuclei/100 µm, $P \leq 0.01$). The density of PR nuclei was not different between gRNA^{CNTRL} and untreated groups ($P = 0.41$) (**Figure 5b**). Visual acuity assessed at P39 by optokinetic response was 53% higher from gRNA^{TRGT} compared with that of gRNA^{CNTRL} treatment (0.185 versus 0.121 cycles/degree, respectively; **Figure 5c**). By using the contralateral eye of individual animals as internal controls, visual acuity was 35% higher in the gRNA^{TRGT}-treated eye compared with the fellow eye in individual animals, whereas, gRNA^{CNTRL}-injection reduced visual acuity by 2.3% compared to the contralateral untreated eye (**Figure 5d**).

DISCUSSION

These data collectively provide proof of principle for *in vivo* allele-specific ablation using CRISPR/Cas9 to prevent inherited retinal degeneration. The selective ablation of *Rho*^{S334} had prevented RHO^{S334} accumulation at PR cell bodies in the ONL and restored RHO^{WT} trafficking to outer segments, which prevented retinal degeneration and preserved visual acuity. Eliminating RHO^{S334} expression generated blunt transition areas at which markedly preserved retinal areas adjoined those with advanced degeneration. These transition regions likely represent the physical extent to which gRNA^{TRGT} transfection had reached, as mCherry expression shared the same demarcation (**Figures 3a** and **Figures 4i,j**). The observation that mCherry expression was not observed in all rescued PRs is likely attributable to the episomal nature of the plasmids and the reduced efficiency of the cytomegalovirus promoter (driving mCherry) compared to that of Chicken β-actin-derivative (driving Cas9).[17] Thus, mCherry expression likely underestimated the total number of PRs in which Cas9/gRNA^{TRGT} was active and therefore the number of PRs in which the *Rho*^{S334} ablation-mediated rescue had occurred.

This assertion is consistent with the S334ter-3 model, in which the expression of *Rho*^{S334} is exclusive to (rod) PRs and instigates cell autonomous apoptotic signaling, suggesting that *Rho*^{S334} ablation is the only manner by which phenotypic rescue could have been achieved with gRNA^{TRGT} treatment. Furthermore, since PRs possess a single copy of the *Rho*^{S334} transgene, its ablation is absolute for conferring PR survivability. Whether this permanent genomic change confers long-term PR survival in a degenerative milieu will require sequential analysis of gRNA^{TRGT}-treated retinas. Toward this goal, PR loss was shown to be halted in an inducible transgenic model of autosomal recessive RP, even at advanced stages of degeneration.[18] Furthermore, a translational proof-of-concept study using gene replacement in a canine model of X-lined RP demonstrated the feasibility of long-term arrest of PR loss.[19] These studies support the possibility of long-term vision rescue following *in vivo* gene correction.

With regard to visual function assessment, optomotor reflexes were significantly preserved from a single gRNA^{TRGT} treatment 39 days prior, compared with controls. Differences in visual function were not detected by electroretinography, however, electroretinography sensitivity is limited for detecting focal retinal activity

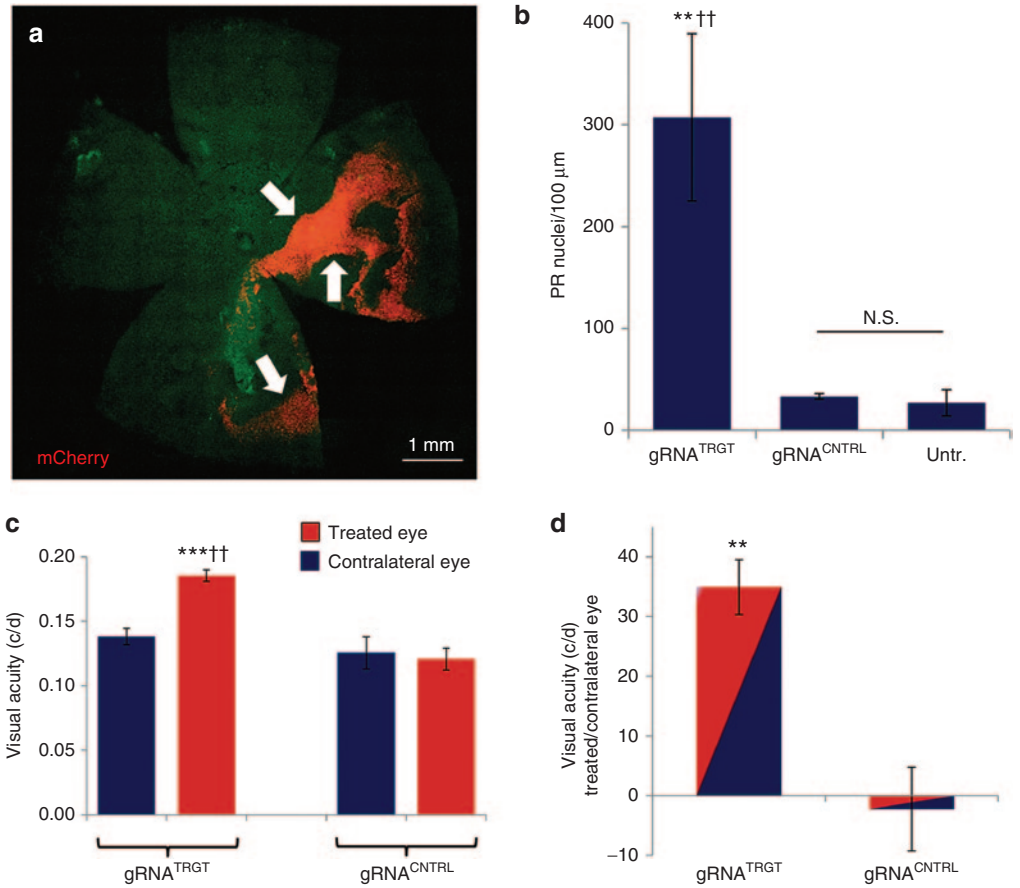

Figure 5 PR rescue by gRNA^{TRGT} treatment corresponded with vision rescue. (**a**) Fluorescent microscopy montage image shows mCherry^{+} reporter distribution (arrows) of gRNA^{TRGT} vector in a retinal flat-mount at P33 calculated at 29% of total retina area by NIH ImageJ analysis. (**b**) By retinal cross-section, mCherry^{+} regions from gRNA^{TRGT} treatment contained significantly more PR nuclei than the mCherry^{+} regions from gRNA^{CNTRL} treatment, or comparable regions from untreated control areas (gRNA^{TRGT}: 307±82 PR nuclei/100 µm, $N = 5$ versus gRNA^{CNTRL}: 33±3, $^{**}P \leq 0.01$, $N = 3$ versus Untreated: 27±13, $^{††}P \leq 0.01$, $N = 4$). (**c**) Visual acuity (optokinetic response) was significantly higher from gRNA^{TRGT} treatment at P39, than from gRNA^{CNTRL} treatment (gRNA^{TRGT}: 0.185±0.008 c/d, $N = 5$ versus gRNA^{CNTRL}: 0.121±0.009 c/d, $N = 4$, $^{††}P \leq 0.01$). Visual acuity in gRNA^{TRGT}-treated eyes was significantly higher than in untreated contralateral eyes (Treated: 0.185±0.008 versus Contralateral: 0.138±0.006 c/d, $N = 5$, $^{***}P \leq 0.001$). Visual acuity in eyes injected with gRNA^{CNTRL} was not different from that of contralateral noninjected eyes (Treated: 0.121±0.009 versus Contralateral: 0.121±0.012 c/d, $N = 4$, $P = 0.763$). (**d**) By using the fellow eyes of individual animals as internal controls, the higher visual acuity from gRNA^{TRGT} treatment represented a 35±4.6% increase, compared to a 2.3±0.7% decrease with gRNA^{CNTRL} injection ($P < 0.01$). c/d = cycles/degree. All values represent mean ± SEM. N.S., not significant; PR, photoreceptor.

and may not represent an appropriate test for our experimental approach. Translational limitations of the current methods are technical in nature and greater functional improvement may be obtained through alternative methods to maximize retinal transfection and genetic correction. For example, the use of shorter Cas9 orthologs, such as *Staphylococcus aureus* (~3.3 kb)[20,21] with short universal tRNA promoter,[22] will allow for efficient vector packaging into adeno-associated viral particles. Alternatively, direct delivery of Cas9 protein/gRNA complexes *in vivo* would also minimize the duration of endonuclease activity and therefore the risk for off-target cleavage events without compromising targeted cleavage efficiency,[23] a critical consideration in the context of using genomic ablation as therapy.

The first *in vivo* functional correction of an inherited dominant mutation using CRISPR, shown here, provides proof-of-concept that CRISPR/Cas9 can be used to treat inherited adRP. Selective ablation of a dominant allele was achieved by targeting a PAM unique to the *Rho*^{S334} transgene, which differed from the *Rho*^{WT} sequence by a single nucleotide. adRP-linked missense mutations that likewise create targetable monoallelic PAM sequences have been identified in patients (**Supplementary Table S1**), who may thus represent the candidate population for ablation therapy to achieve phenotypic rescue. The challenge of generating targeted therapies for diseases with mutational heterogeneity may be addressed by altering the PAM specificity of Cas through rational-design engineering[24] or by using noncanonical Cas enzymes.[25] Such efforts may broaden the number of targetable mutations and, thereby, expand the treatable pool of patients with degenerative diseases of the retina, and possibly other tissues.

MATERIALS AND METHODS

Cas9/gRNA vector design. gRNAs were cloned into px330 vectors (Life Technologies, Carlsbad, CA) via BbsI restriction enzyme sites upstream of the scaffold gRNA sequence and the mCherry reporter (Addgene, Cambridge, MA) was cloned downstream of the *Cas9* transcript, which was under constitutive expression by cytomegalovirus promoter.

Cas9 cleavage efficiency determination. *Rho*^{S334}-selective disruption was confirmed in PRs that were fluorescence-activated cell sorting-isolated by mCherry^{Hi} and intermediate/low mCherry^{Lo} expression and was confirmed absent in mCherry-negative (mCherry^{Neg}) PRs from three animals (**Supplementary Figure S2**). Cleavage efficiency was calculated from the indel frequency among bacterial clones transfected with DNA from mCherry-isolated cells. Genomic DNA was extracted from mCherry^{+} PRs or MSCs^{S334} and subjected to PCR amplification using primers that flanked the predicted Cas9 cut site regions. Amplicons from on- and off-target cleavage sites were ligated into plasmids (T-vector Cloning Kit, Life Technologies, Carlsbad, CA) and transfected into high-efficiency NEB-α *E. coli* (New England BioLabs, Ipswich, MA) for DNA Sanger sequencing analysis of 21–42 clones from which the ratios of genomic disruptions were used to quantify cleavage efficiency (**Supplementary Table S2**).

Animal procedures. All animal procedures were performed in accordance with the Cedars-Sinai Medical Center's Institutional Animal Care and Use Committee and the ARVO Statement for the Use of Animals in Ophthalmic and Vision Research. Injection methods used were slightly modified from a previous published protocol.[26] S334ter-3 P0 rats were anesthetized on ice for 5 minutes, and 1 µl of plasmid DNA (6–7.4 µg/µl) was diluted 0.1× (v/v) with Fast-Green DNA dye and subretinally injected by floating needle into S334ter-3 rats. Subsequent electroporation of plasmid DNA consisted of five pulses at 115 mV with 50-ms duration and 950-ms intervals, using a longitudinal sweeping motion with 7-mm Platinum Tweezertrodes lubricated with conductance enhancing SignaGel (ECM 830 System, Harvard Apparatus, Holliston, MA). Positive charge was generated over the injected eye. Pups were allowed to recover on a heating pad.

Cell sources and cell processing. Eyes were surgically removed and kept in 4–6 °C phosphate-buffered saline (pH 7.4) for ~30 minutes. Retinas were dissected and subjected to single-cell dissociation by incubating for 20 minutes at 37 °C in enzymatic digestion solution consisting of Ca^{2+}/Mg^{2+}-free phosphate-buffered saline, 20 U/ml papain, and 0.5 mmol/l L-cysteine (Worthington Biochemical Corp., Lakewood, NJ). mCherry^{+} retinal cells were sorted (FACSAria III, BD Biosciences, Franklin Lakes, NJ) into 1.7 ml DNase-free tubes (Eppendorf, Hamburg, Germany) containing 4 °C phosphate-buffered saline and subjected to genomic DNA extraction (Purelink Genomic DNA Mini Kit, Life Technologies). MSCs^{S334} were derived from adult rats as previously described.[27] Briefly, the femurs of 6–8-week-old S334ter-3 rats were flushed with Dulbecco's Modified Eagle Medium (Life Technologies), gently triturated in 5 ml syringe, passed through a 40 µm strainer, centrifuged at 600 × *g* for 10 minutes, plated at 1,000 cells/cm^2 onto T75 tissue culture flasks (Corning, Corning, NY) in growth medium consisting of Dulbecco's Modified Eagle Medium containing 10% fetal bovine serum (Atlanta Biologicals, Lawrenceville, GA), 100 U/ml penicillin, and 100 µg/ml streptomycin sulfate (Life Technologies), and cultured in a humidified incubator at 37° and 5% CO_2. Nonadherent cells were removed by media change after 24 hours.

Immunofluorescent staining and confocal microscopy. Eyes were enucleated and fixed (4% paraformaldehyde in phosphate-buffered saline) for 1 hour and embedded in OCT Compound (Sakura Finetek, Torrance, CA) after 30% sucrose infiltration. Select eyes were prepared for retinal whole-mount dissection to assess mCherry distribution prior to embedding. Frozen transverse 10-µm-thick retinal sections were histologically stained (0.4% cresyl violet acetate, Sigma Aldrich, St. Lois, MO) or immunolabeled with antibodies generated against: Cone arrestin (rabbit polyclonal, 1:1,000, AB15282, Millipore, Billerica, MA), protein kinase C-α (rabbit polyclonal, 1:5,000, P4334, Sigma), Synaptophysin (mouse clone SVP-38, 1:2,000, Millipore MAB368), Rhodopsin (C-terminal, clone 1D4, 1:100, Millipore MAB5356 or N-terminal, 1:100, clone RET-P1, Millipore MAB5316). Alexa-Fluor-488 (1:500; Life Technologies) was used to visualize sections along with nuclear counterstain (49,69-diamidino-2-phenylindole, Vector Laboratories, Burlingame, CA). Images were captured by confocal microscopy (Eclipse C1si, Nikon Instruments, Melville, NY) and morphology, mCherry distribution, and PR nuclei counts were analyzed by Image J software (NIH, Bethesda, MD).

Visual function assessment. Animals were tested for spatial visual acuity by OptoMotry testing apparatus (CerebralMechanics, Lethbridge, Alberta, Canada) as previously described,[28] in which four computer monitors are arranged in a square to project a 3D virtual space of a rotating cylinder lined with vertical sine wave grating. Unrestrained animals on a center platform tracked the projected image of rotating grating with reflexive head movements. The spatial frequency of the grating (cycles per degree) was centered on the rats' viewing position, and maximal acuity ascertained by increasing the grating frequency at psychophysics staircase progression until the tracking response was lost.

Statistical significance. Student's *t*-tests were performed using two-tailed distribution, and two-sample unequal variance (heteroscedastic) to compare optokinetic response cycles/degree values from treated versus untreated eyes of individual animals, as well as between animals of treatment groups; gRNA^{TRGT} (N = 5) and gRNA^{CNTRL} (N = 4). Contralateral noninjected eyes served as untreated controls. Error bars indicate standard error mean. Statistical significance: $^{**}P \leq 0.01$, $^{\dagger\dagger}P \leq 0.01$, $^{***}P \leq 0.001$.

SUPPLEMENTARY MATERIAL

Figure S1. PR degeneration characteristics in untreated S334ter-3 rats.

Figure S2. Confirmation of *Rho*^{S334} disruption from gRNA^{TRGT} treatment in three rats.

Figure S3. Histological evaluation of phenotype rescue following *Rho*^{S334}-selective ablation.

Table S1. Dominant mutations that generate novel PAM sequences identified in patients.

Table S2. Efficiency and off-target genomic cleavage detection in PRs.

ACKNOWLEDGMENTS

The authors thank Lin Shen of Regenerative Medicine Institute for experimental assistance, Laura Dieu and Patricia Lin of the Cedars-Sinai Flow Cytometry Core, and Seigo Hatada and Soshana Svendsen for manuscript review. Financial support was provided by the Cedars-Sinai Board of Governors Regenerative Medicine Institute, Fight for Sight Foundation (FFS-PD-14–053.R1), and NEI (EY020488). S.W., B.L., W.L., and B.B. are coinventors on US provisional patent applications 62/149,468 and 62/147,981; W.L. conceived of the project; B.B. assembled the figures and drafted the manuscript; W.L., B.B., and S.W. designed and conducted experiments; K.J.K., B.L., Y.T., and M.K.J. conducted experiments; R.L. and A.A.A. assisted with electroporation; J.J.B. provided reagents and use of equipment; and C.N.S. provided funding and critical review.

REFERENCES

1. Petrs-Silva, H and Linden, R (2014). Advances in gene therapy technologies to treat retinitis pigmentosa. *Clin Ophthalmol* **8**: 127–136.
2. Wilson, JH and Wensel, TG (2003). The nature of dominant mutations of rhodopsin and implications for gene therapy. *Mol Neurobiol* **28**: 149–158.
3. Rossmiller, B, Mao, H and Lewin, AS (2012). Review: gene therapy in animal models of autosomal dominant retinitis pigmentosa. *Molecular Vision* **18**: 2479–2496.
4. LaVail, MM, Yasumura, D, Matthes, MT, Drenser, KA, Flannery, JG, Lewin, AS *et al.* (2000). Ribozyme rescue of photoreceptor cells in P23H transgenic rats: long-term survival and late-stage therapy. *Proc Natl Acad Sci USA* **97**: 11488–11493.
5. Lewin, AS, Drenser, KA, Hauswirth WW, Nishikawa S, Yasumura D, Flannery JG *et al.* (1998) Ribozyme rescue of photoreceptor cells in a transgenic rat model of autosomal dominant retinitis pigmentosa. *Nat Med* **8**: 967–971.
6. Mussolino, C, Sanges, D, Marrocco, E, Bonetti, C, Di Vicino, U, Marigo, V *et al.* (2011). Zinc-finger-based transcriptional repression of rhodopsin in a model of dominant retinitis pigmentosa. *EMBO Mol Med* **3**: 118–128.
7. Concepcion, F, Mendez, A and Chen, J (2002). The carboxyl-terminal domain is essential for rhodopsin transport in rod photoreceptors. *Vision Res* **42**: 417–426.
8. McGill, TJ, Prusky, GT, Luna, G, LaVail, MM, Fisher, SK and Lewis, GP (2012). Optomotor and immunohistochemical changes in the juvenile S334ter rat. *Exp Eye Res* **104**: 65–73.
9. Chen, J, Makino, CL, Peachey, NS, Baylor, DA and Simon, MI (1995). Mechanisms of rhodopsin inactivation *in vivo* as revealed by a COOH-terminal truncation mutant. *Science* **267**: 374–377.

10. Sung, CH, Makino, C, Baylor, D and Nathans, J (1994). A rhodopsin gene mutation responsible for autosomal dominant retinitis pigmentosa results in a protein that is defective in localization to the photoreceptor outer segment. *J Neurosci* **14**: 5818–5833.
11. Martinez-Navarrete, G, Seiler, MJ, Aramant, RB, Fernandez-Sanchez, L, Pinilla, I and Cuenca, N (2011). Retinal degeneration in two lines of transgenic S334ter rats. *Exp Eye Res* **92**: 227–237.
12. Pennesi, ME, Nishikawa, S, Matthes, MT, Yasumura, D and LaVail, MM (2008). The relationship of photoreceptor degeneration to retinal vascular development and loss in mutant rhodopsin transgenic and RCS rats. *Exp Eye Res* **87**: 561–570.
13. Mendes, HF, van der Spuy, J, Chapple, JP and Cheetham, ME (2005). Mechanisms of cell death in rhodopsin retinitis pigmentosa: implications for therapy. *Trends Mol Med* **11**: 177–185.
14. Green, ES, Menz, MD, LaVail, MM and Flannery, JG (2000). Characterization of rhodopsin mis-sorting and constitutive activation in a transgenic rat model of retinitis pigmentosa. *Invest Ophthalmol Vis Sci* **41**: 1546–1553.
15. Retina International. Retina International Mutation Database <http://www.retina-international.org/sci-news/databases/mutation-database>.
16. Matsuda, T and Cepko, CL (2007). Controlled expression of transgenes introduced by *in vivo* electroporation. *Proc Natl Acad Sci USA* **104**: 1027–1032.
17. Allocca, M, Mussolino, C, Garcia-Hoyos, M, Sanges, D, Iodice, C, Petrillo, M *et al.* (2007). Novel adeno-associated virus serotypes efficiently transduce murine photoreceptors. *J Virol* **81**: 11372–11380.
18. Koch, SF, Tsai, YT, Duong, JK, Wu, WH, Hsu, CW, Wu, WP *et al.* (2015). Halting progressive neurodegeneration in advanced retinitis pigmentosa. *J Clin Invest* **125**: 3704–3713.
19. Beltran, WA, Cideciyan, AV, Iwabe, S, Swider, M, Kosyk, MS, McDaid, K *et al.* (2015). Successful arrest of photoreceptor and vision loss expands the therapeutic window of retinal gene therapy to later stages of disease. *Proc Natl Acad Sci USA* **112**: E5844–E5853.
20. Ran, FA, Cong, L, Yan, WX, Scott, DA, Gootenberg, JS, Kriz, AJ *et al.* (2015). *In vivo* genome editing using *Staphylococcus aureus* Cas9. *Nature* **520**: 186–191.
21. Kleinstiver, BP, Prew, MS, Tsai, SQ, Nguyen, NT, Topkar, VV, Zheng, Z *et al.* (2015). Broadening the targeting range of *Staphylococcus aureus* CRISPR-Cas9 by modifying PAM recognition. *Nat Biotechnol* **33**: 1293–1298.
22. Mefferd, AL, Kornepati, AV, Bogerd, HP, Kennedy, EM and Cullen, BR (2015). Expression of CRISPR/Cas single guide RNAs using small tRNA promoters. *RNA* **21**: 1683–1689.
23. Zuris, JA, Thompson, DB, Shu, Y, Guilinger, JP, Bessen, JL, Hu, JH *et al.* (2015). Cationic lipid-mediated delivery of proteins enables efficient protein-based genome editing *in vitro* and *in vivo*. *Nat Biotechnol* **33**: 73–80.
24. Kleinstiver, BP, Prew, MS, Tsai, SQ, Topkar, VV, Nguyen, NT, Zheng, Z *et al.* (2015). Engineered CRISPR-Cas9 nucleases with altered PAM specificities. *Nature* **523**: 481–485.
25. Anders, C, Niewoehner, O, Duerst, A and Jinek, M (2014). Structural basis of PAM-dependent target DNA recognition by the Cas9 endonuclease. *Nature* **513**: 569–573.
26. Matsuda, T and Cepko, CL (2004). Electroporation and RNA interference in the rodent retina *in vivo* and *in vitro*. *Proc Natl Acad Sci USA* **101**: 16–22.
27. Egles, C, Wang, S, Lu, B, Girman, S, Duan, J, McFarland, T *et al.* (2010) Non-invasive stem cell therapy in a rat model for retinal degeneration and vascular pathology. *PLoS ONE* **5**: e9200.
28. Tsai, Y, Lu, B, Bakondi, B, Girman, S, Sahabian, A, Sareen, D *et al.* (2015). Human iPSC-derived neural progenitors preserve vision in an AMD-like model. *Stem Cells* **33**: 2537–2549.